Visible Upconversion in Rare Earth Ion-Doped Gd_2O_3 Nanocrystals

Hai Guo,[†,‡] Ning Dong,[‡] Min Yin,[†,‡] Weiping Zhang,[*,‡] Liren Lou,[‡] and Shangda Xia[‡]

Structure Research Laboratory, and Department of Physics, University of Science and Technology of China, Academia Sinica, 230026 Hefei, Anhui, People's Republic of China

Received: May 5, 2004; In Final Form: September 7, 2004

Rare earth ions (Tm^{3+}, Er^{3+}, and Yb^{3+})-doped cubic Gd_2O_3 nanocrystals were prepared by a simple sol−gel method. Raman and FT-IR spectra were measured to evaluate the vibrational feature of the samples. Under 980 nm laser excitation, blue (488 nm), green (564 nm), and red (661 nm) upconversion has been recorded in Gd_2O_3:Tm+Yb and Gd_2O_3:Er (Gd_2O_3:Er+Yb), respectively. A great enhancement of red emission and diminishment of green emission of Er^{3+} in Gd_2O_3:Er+Yb have been observed. Laser power and doping concentration dependence of the upconverted emissions were studied to understand the upconversion mechanisms. Excited absorption and energy-transfer processes are discussed as the possible mechanisms for the visible emissions.

1. Introduction

There has been an intense interest recently in the investigation of upconversion luminescence for a wide range of applications, such as all-solid compact laser devices, infrared quantum counter detectors, fluorescent labels for sensitive detection of biomolecules, and optical data storage.[1−18] Erbium ion is an excellent candidate for upconversion as its metastable levels $^4I_{9/2}$ and $^4I_{11/2}$ can be conveniently populated by commercial low-cost high-power near-infrared laser diodes.[1−6,10−14] The sensitization effect of Yb^{3+} ions is well known for increasing the optical pump efficiency of luminescent centers. This is because Yb^{3+} ions have a large absorption cross section around 980 nm and can efficiently transfer the excitation energy to other rare earth ions.[2−4,15,16]

On the other hand, during recent years, the preparation and the investigation of optical properties of nanocrystals have attracted considerable interest in both fundamental research and practical applications.[7−14,18−21] In the field of practical phosphors, there is an ongoing search for luminescent materials with higher efficiency and smaller size. Plenty of the work was focused on rare earth ions-doped Y_2O_3 nanocrystals.[8−12,20−21]

Similar to Y_2O_3, gadolinium oxide (Gd_2O_3) is a promising host matrix for upconversion because of its good chemical durability, thermal stability, and low phonon energy (phonon cutoff ≈ 600 cm^{-1}). The former character makes it suitable for practical application, and the later one would increase the possibility of radiative transitions and in turn result in a high quantum yield of upconverion process. In addition, Gd_2O_3 can be easily doped with rare earth ions, which means high concentration doping is possible. Yet there are only few reports on the upconversion of rare earth ions-doped Gd_2O_3 nanocrystals.[7,22]

In the present work, cubic Gd_2O_3:Tm (GOT), Gd_2O_3:Tm+Yb (GOTY), Gd_2O_3:Er (GOE), and Gd_2O_3:Er+Yb (GOEY) nanocrystals were prepared by a simple sol−gel method. The structural properties of samples were characterized by X-ray diffraction (XRD), transmission electron microscopy (TEM), Raman spectroscopy, and Fourier transform infrared (FT-IR) spectroscopy. Under excitation into the $^2F_{5/2}$ level of Yb^{3+} and the $^4I_{11/2}$ level of Er^{3+} ions by 980 nm laser, the upconverted luminescence of GOTY, GOE, and GOEY was recorded. The mechanisms were studied through power and concentration dependence of upconverted emissions. The energy-transfer processes from Yb^{3+} to Er^{3+} and Tm^{3+} ions were also discussed.

2. Experimental Procedure

GOT, GOTY, GOE, and GOEY nanocrystals with different doping concentration were prepared by a simple sol−gel method.[7] Dried gadolinium acetate ($Gd(OAC)_3$) and rare earth nitrate were used as the starting materials. Methoxyethanol (HORE) and diethylenetriamine (DETA) were adopted as solvent and complexant, respectively. First, $Gd(OAC)_3$ was mixed with HORE and DETA. After the mixture was stirred for 2 h, the proper amount of water and rare earth nitrate aqueous solution were added into the precursor solution and stirred for another 4 h. Enough water was then added into the solution to form gel. The dried gel, obtained by drying the gel at 80 °C for 20 h, was heated at 200 °C for 4 h. At last, products were obtained after sintering at 700−900 °C for 1 h.

X-ray diffraction (XRD) was carried out on a MAC Science Co. Ltd. (Japan) MXP18AHF X-ray diffraction apparatus with Cu Kα radiation. Morphology study of the Gd_2O_3 nanoparticles was performed on a Hitachi H-800 transmission electron microscope. The infrared absorption spectra were recorded in the range of 4000−400 cm^{-1} with a Magna-IR 750 Fourier transform infrared (FT-IR) spectrometer. The Raman spectra and Stokes emission spectra were measured and analyzed by using a Jobin-Yvon LABRAM-HR confocal laser micro-Raman spectrometer system equipped with an Ar ion 514.5 nm laser.

Blue, green, and red upconversion emissions, excited by a 980 nm diode laser, were dispersed by a Jobin-Yvon HRD1 double monochromator and were detected by a Hamamatsu R456 photomultiplier. The signal was analyzed by an EG&G 7265 DSP lock-in amplifier and stored into computer memories. All of the measurements were carried out at room temperature.

* Corresponding author. Phone: 86-551-3606577. Fax: 86-551-3601073. E-mail: wpzhang@ustc.edu.cn.
† Structure Research Laboratory.
‡ Department of Physics.

10.1021/jp048072q CCC: $27.50
Published on Web 11/20/2004

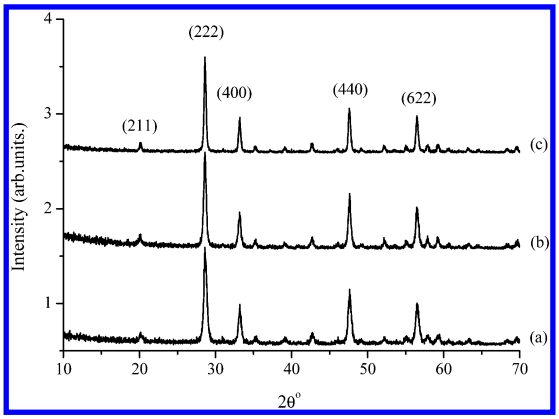

Figure 1. Powder X-ray diffraction patterns of Gd_2O_3 nanoparticles heat-treated at (a) 700, (b) 800, and (c) 900 °C for 1 h.

3. Results and Discussion

3.1. Structural Properties. Figure 1 is the XRD patterns of the Gd_2O_3 powders heat-treated at a temperature of 700−900 °C. The result shows that the samples crystallized in cubic Gd_2O_3 with spatial group *Ia*3 (JCPDS card No. 11-0604). The crystallite size D can be estimated by following Scherrer's equation:[7]

$$D = k\lambda/\beta \cos\theta \qquad (1)$$

where $k = 0.89$, λ(nm) represents the wavelength of Cu Kα radiation, θ is the Bragg angle of the X-ray diffraction peak, and β stands for the corrected half width of the diffraction peak. The estimated crystallite size increases with the heat-treated temperature. For a sample sintered at 700, 800, and 900 °C, the crystallite sizes are 25, 29, and 41 nm, respectively.

The TEM image of the Gd_2O_3 nanoparticles[7] (not shown here) shows that the size distribution is broad and the average diameter is in good agreement with that estimated by Scherrer's equation.

Raman spectroscopy can be used to characterize the phonon energy of materials. The Stokes Raman spectrum ($\lambda_{ex} = 514.5$ nm) of Gd_2O_3 nanoparticles sintered at 900 °C (not shown here) shows an intense peak at 359.3 cm^{-1} and four weak peaks around 117.2, 313.5, 441.4, and 567.6 cm^{-1}. These results are in fair agreement with that of bulk cubic Gd_2O_3.[23]

Upconversion efficiency is governed principally by the nonradiative process of the materials. The multi-phonon nonradiative decay rate can be expressed by the following energy gap law:[24]

$$W_n = W_o[1 - \exp(-h\upsilon/kT)]^{-n} \qquad (2)$$

where W_n is the rate at temperature T, W_0 is the rate at 0 K, $n = \Delta E/h\upsilon$, ΔE is the energy gap between the levels involved, and υ is the relevant phonon's frequency. When ΔE is equal to or less than 4−5 times the high-energy phonons, the multi-phonon nonradiative relaxation becomes competitive with the radiative processes.

Atomic groups with high vibrational frequency will increase the nonradiative relaxation rate and hence decrease upconversion efficiency. The greatest phonon energy of Gd_2O_3 nanocrystals is about 600 cm^{-1}. However, CO and OH groups with high-energy vibrations may still exist in the samples because the sol−gel process always involves hydrolysis, polymerization, oxidation, and decomposition processes. To obtain high upconversion efficiency, CO and OH groups must be removed from the samples.

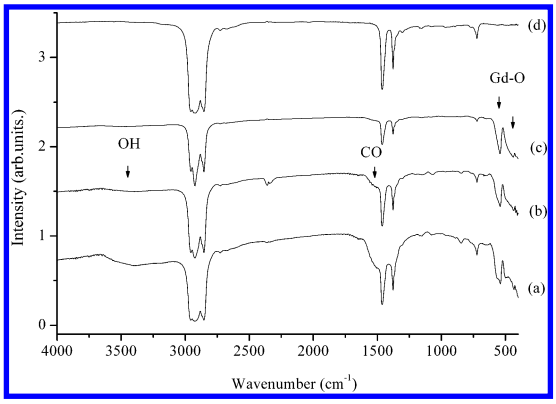

Figure 2. FT-IR spectra of Gd_2O_3 nanoparticles heat-treated for 1 h at (a) 700, (b) 800, and (c) 900 °C, and (d) pure paraffin.

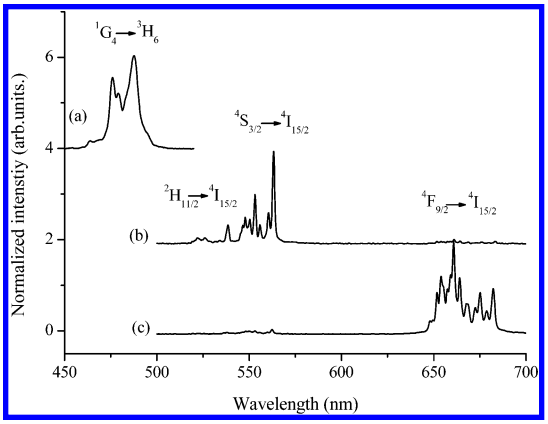

Figure 3. Upconversion spectra of rare earth ions-doped Gd_2O_3 nanoparticles. (a) Gd_2O_3:Tm (1%)+Yb (5%); (b) Gd_2O_3:Er (1%); (c) Gd_2O_3:Er (1%)+Yb (10%). $\lambda_{ex} = 980$ nm.

Figure 2 presents the FT-IR transmission spectra of Gd_2O_3 sintered at 700 (a), 800 (b), and 900 °C (c) in paraffin pellets and pure paraffin (d) as a reference. The bands around 542 and 440 cm^{-1} are assigned to the Gd−O vibration of cubic Gd_2O_3.[25] It can be seen that the absorption bands of OH (around 3400 cm^{-1}) and CO groups (around 1500 cm^{-1}) become weaker with increasing sintering temperature and nearly disappear after heating at 900 °C. This result indicates that there are no OH or CO groups in the Gd_2O_3 nanocrystals sintered at 900 °C, implying that such samples may have higher upconversion efficiency. Therefore, the upconversion investigation was conducted only on samples sintered at 900 °C.

3.2. Upconversion Spectra. Figure 3 is the normalized upconversion spectra of (a) Gd_2O_3:Tm (1%)+Yb (5%), (b) Gd_2O_3:Er (1%), and (c) Gd_2O_3:Er (1%)+Yb (10%) under 980 nm laser excitation. The blue emission near 488 nm comes from the $^1G_4 \rightarrow {}^3H_6$ transition of Tm^{3+} ions.[15−16] The sharp peaks in the green region of 520−541 and 545−565 nm are assigned to the transitions $^2H_{11/2} \rightarrow {}^4I_{15/2}$ and $^4S_{3/2} \rightarrow {}^4I_{15/2}$ of Er^{3+} ions, respectively, while the peaks in the red region of 645−686 nm correspond to the $^4F_{9/2} \rightarrow {}^4I_{15/2}$ transition.[1−6] A wide spectrum of colors, including white, would be produced by appropriate mixing of these three primary colors.

The concentration dependence of upconverted emission was investigated and is shown in Figures 4 and 5. Figure 4 tell us that emission intensity and relative intensity of red emission increase with Er^{3+} concentration. Figure 5 gives the upconversion spectra of GOEY nanoparticles with different Yb^{3+} ion concentration. The results show that green emission intensity decreases with increasing Yb^{3+} concentration while red intensity increases. This behavior is quite different from the reports on

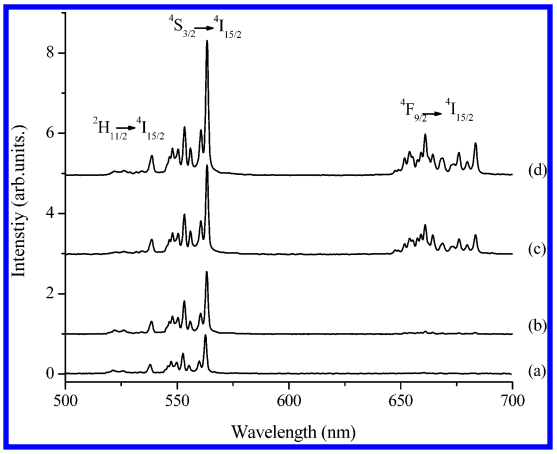

Figure 4. Upconversion spectra of Er^{3+}-doped Gd_2O_3 nanoparticles with different Er^{3+} concentration: (a) 0.5%, (b) 1%, (c) 3%, (d) 6%.

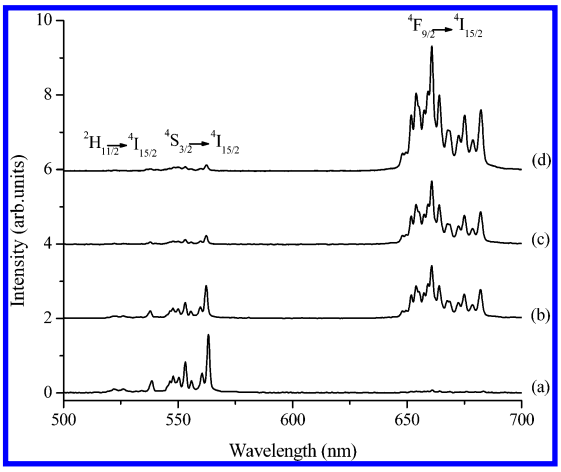

Figure 5. Upconversion spectra of Er^{3+}/Yb^{3+}-doped Gd_2O_3 nanoparticles with different Yb^{3+} concentration: (a) 0%, (b) 2%, (c) 5%, (d) 10%.

Er^{3+}/Yb^{3+}-codoped chalcogenide glass, lead oxyfluorosilicate glass, and lead−niobium−germanate glass,[2−4] but a similar result is observed in Er^{3+}/Yb^{3+}-codoped Y_2O_3 nanocrystals.[8]

To understand the upconversion mechanisms, the upconversion emission intensity I was measured as a function of the pump power P. For the upconversion process, I is proportional to the nth power of P, that is:

$$I \propto P^n \tag{3}$$

where n is the number of pump photons absorbed per upconverted photon emitted.[1−3] A plot of log I versus log P yields a straight line with slope n. The result is shown in Figure 6 for different samples. For the sample of Gd_2O_3:Tm (1%)+Yb (5%) (Figure 3a), the slope n was 2.90 ± 0.14 for blue emission ($^1G_4 \rightarrow {}^3H_6$), which indicates that the blue upconversion emission is a three-photon process. For the sample of Gd_2O_3:Er (6%) (Figure 4d), the obtained n was 2.06 ± 0.05 and 2.07 ± 0.09 for green ($^4S_{3/2} \rightarrow {}^4I_{15/2}$) and red emissions ($^4F_{9/2} \rightarrow {}^4I_{15/2}$), respectively. The slope n for red emission of Gd_2O_3:Er (1%)+Yb (10%) (Figure 5d) was 1.73 ± 0.04. These results show that the two-photon process is responsible for green and red upconversion.

The excited states for upconversion can be populated by several well-known mechanisms: (1) excited-state absorption (ESA), (2) energy transfer (ET), and (3) photon avalanche.[12] Photon avalanche was ruled out as a possible mechanism for upconversion because no inflection point was observed in the power study.[12] Figure 7 pictures the energy level diagram of

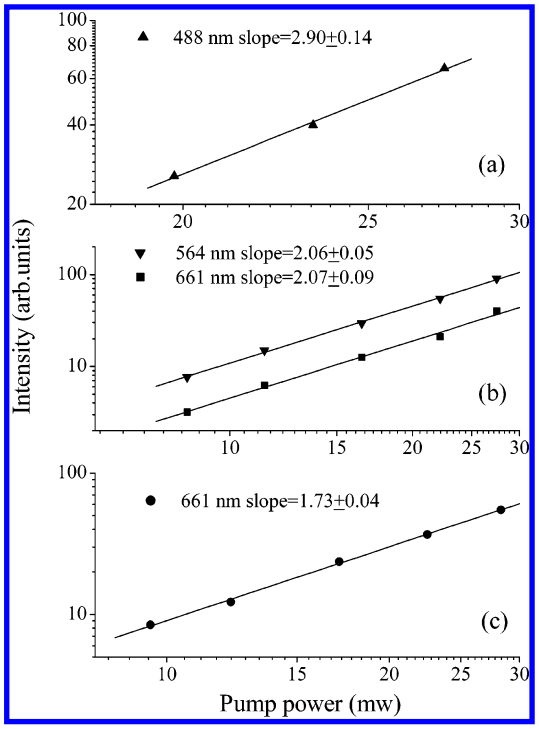

Figure 6. Dependence of the upconversion emission intensity on excitation power in different samples. (a) Gd_2O_3:Tm (1%)+Yb (5%); (b) Gd_2O_3:Er (6%); and (c) Gd_2O_3:Er (1%)+Yb (10%).

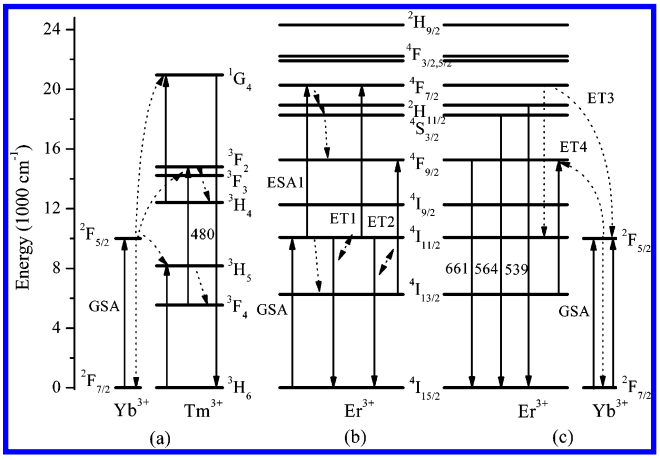

Figure 7. Energy level diagrams of rare earth ions in Gd_2O_3 and upconversion mechanisms.

Tm^{3+}, Er^{3+}, and Yb^{3+} ions as well as the probable upconversion mechanisms accounting for the blue, green, and red emissions under 980 nm excitation.

Gd_2O_3:Tm^{3+} does not show blue upconversion because Tm^{3+} ions cannot absorb 980 nm photons (not shown here). For sample codoped with Yb^{3+} ions (Figure 3a), Yb^{3+} ions are pumped to the $^2F_{5/2}$ level by absorbing the 980 nm photons, and the Tm^{3+} ions are excited into the $^1G_4$ level through three-step energy transfer:[15−16] (1) a Tm^{3+} ion is excited into the $^3H_5$ level by the energy-transfer process, $^3H_6$ (Tm) + $^2F_{5/2}$ (Yb) → $^3H_5$ (Tm) + $^2F_{7/2}$ (Yb), and the Tm^{3+} ion then relaxes into the $^3F_4$ level; (2) the same Tm^{3+} ion is further excited into the $^3F_2$ level by another energy-transfer process, $^3F_4$ (Tm) + $^2F_{5/2}$ (Yb) → $^3F_2$ (Tm) + $^2F_{7/2}$ (Yb), and then relaxes to the lower metastable $^3H_4$ state; and (3) a third excited Yb^{3+} ion transfers its excitation energy to this Tm^{3+} ion and excites it from the $^3H_4$ level to $^1G_4$ state ($^3H_4$ (Tm) + $^2F_{5/2}$ (Yb) → $^1G_4$ (Tm) + $^2F_{7/2}$ (Yb)). The $^1G_4 \rightarrow {}^3H_6$ transition of Tm^{3+} ions results in blue emissions around 488 nm.

TABLE 1: Stokes Emission Intensity of GOEY Samples[a]

intensity	green	red	red vs green
Gd_2O_3:Er (1%)	6269	504	0.08
Gd_2O_3:Er (1%)+Yb (2%)	442	233	0.53
Gd_2O_3:Er (1%)+Yb (10%)	100	153	1.53

[a] The ET3 process shown in Figure 7 causes the decrease in green emission intensity.

For GOE samples (Figure 7b), Er^{3+} ions are excited from the ground state to the $^4I_{11/2}$ level by absorbing one 980 nm laser photon (GSA). The ions in the $^4I_{11/2}$ level sequentially absorb another 980 nm photon and are raised to the $^4F_{7/2}$ level. This is an excited-state absorption process, labeled as ESA1 (in Figure 7). The ions in the $^4F_{7/2}$ level undergo multi-phonon relaxation to luminescent $^2H_{11/2}$ and $^4S_{3/2}$ levels. In addition, there is a possible ET route that can also populate these luminescent levels, which is labeled as ET1: $^4I_{11/2} + {}^4I_{11/2} \rightarrow {}^4I_{15/2} + {}^4F_{7/2}$. The luminescent $^4F_{9/2}$ level can be pumped via a nonradiative relaxation through the $^4S_{3/2}$ excited state with a moderate rate given by eq 2. Due to the low phonon cutoff of Gd_2O_3 and the large energy gap ΔE between $^4S_{3/2}$ and $^4F_{9/2}$ levels (3200 cm^{-1}), the nonradiative relaxation rate from $^4S_{3/2}$ level is low, which is confirmed by the weak red emission in low Er^{3+} concentration samples. From the change of relative intensity of red and green emissions in the samples with different Er^{3+} ion concentrations (in Figure 4), it is reasonable to assume that there is another ET process that only populates the $^4F_{9/2}$ level. This ET process may describe as follows: $^4I_{13/2} + {}^4I_{11/2} \rightarrow {}^4F_{9/2} + {}^4I_{15/2}$ (Figure 7: ET2).[1] The populated $^4I_{13/2}$ level may be excited through a multi-phonon nonradiative process from the $^4I_{11/2}$ level and radiative process from upper levels, such as the $^4S_{3/2}$ level.

For GOEY samples, the Er^{3+} ion can be excited from the ground-state $^4I_{15/2}$ to the excited-state $^4I_{11/2}$ by one of the two processes: ground-state absorption and energy transfer from the excited Yb^{3+} ions ($^4I_{15/2}$ (Er) + $^2F_{5/2}$ (Yb) $\rightarrow$ $^4I_{11/2}$ (Er) + $^2F_{7/2}$ (Yb)). The later one dominates the process because the Yb^{3+} ions have a much larger absorption cross section as compared to that of Er^{3+} ions around 980 nm.[2−4] Then, the ions in the $^4I_{11/2}$ level were excited to the $^4F_{7/2}$ level by the ESA1 process. After that, the ions undergo multi-phonon relaxation to luminescent levels $^2H_{11/2}$ and $^4S_{3/2}$. In addition, the contribution of ET1 and ET2 processes to the upconversion emissions in GOEY cannot be rejected. As mentioned above, the upconversion behavior of GOEY samples (Figure 5) is quite different from the reports on Er^{3+}/Yb^{3+}-codoped materials,[2−4] where the green emission intensity increases with increasing Yb^{3+} ions concentration, while in our work, the intensity of green emission decreases with increasing Yb^{3+} ions concentration. Therefore, some new paths different from refs 2−4 must be involved to explain this phenomenon. It was reported that in Er^{3+}/Yb^{3+}-codoped Y_2O_3, an energy-transfer process (ET3), $^4F_{7/2}$ (Er) + $^2F_{7/2}$ (Yb) $\rightarrow$ $^4I_{11/2}$ (Er) + $^2F_{5/2}$ (Yb), occurs to pump the Yb^{3+} to the $^2F_{5/2}$ under 488 nm laser excitation.[11] Therefore, it is reasonable to assume that the ET3 process depopulates the excited $^4F_{7/2}$ level and causes the decrease of green emission intensity. We investigate the effect of Yb^{3+} ions on the Stokes ($\lambda_{ex} = 514.5$ nm) emission intensity of GOEY samples. Under 514.5 nm laser excitation, the Er^{3+} ions were excited to the $^4F_{7/2}$ level and then relax to emitting levels. Table 1 lists the Stokes emission intensity of GOEY samples and shows that, with increasing Yb^{3+} ions concentration, green emission intensity decreases greatly due to the ET3 process. This investigation proved indirectly our former assumption. For red emission, the luminescent $^4F_{9/2}$ level can be pumped via a nonradiative relaxation through the $^4S_{3/2}$ excited state with a quite low rate. These are similar to those of the single Er^{3+} ions-doped samples. With increasing Yb^{3+} ions concentration, the intensity of red emission increases greatly (in Figure 7). Therefore, other energy-transfer process, which will populate the $^4F_{9/2}$ level, must be put forward to account for this phenomenon. A possible way is that the populated $^4I_{13/2}$ level was excited to the $^4F_{9/2}$ level by energy transfer from the excited Yb^{3+} ions (Figure 7 ET4: $^4I_{13/2}$ (Er) + $^2F_{5/2}$ (Yb) $\rightarrow$ $^4F_{9/2}$ (Er) + $^2F_{7/2}$ (Yb)).[2−4]

4. Conclusions

Rare earth ions (Tm^{3+}, Er^{3+}, and Yb^{3+})-doped cubic Gd_2O_3 nanocrystals were prepared by a simple sol−gel method. FT-IR and Raman spectra show that Gd_2O_3 nanocrystals sintered at 900 °C (41 nm in size) may present higher upconversion efficiency because of its low vibrational frequency. Under 980 nm laser excitation, blue (488 nm), green (564 nm), and red (661 nm) upconversion emissions have been observed in Gd_2O_3:Tm+Yb and Gd_2O_3:Er (Gd_2O_3:Er+Yb), respectively. A wide spectrum of colors, including white, would be produced by appropriate mixing of these three primary colors. The laser power dependence on upconverted emissions revealed that three-photon and two-photon processes lead to blue, green, and red emissions, respectively. The doping of Yb^{3+} plays an important role in green and red upconversion of Gd_2O_3:Er+Yb samples. The great enhancement of red emission and diminishment of green emission of Er^{3+} in Gd_2O_3:Er+Yb were caused by ET4 ($^4I_{13/2}$ (Er) + $^2F_{5/2}$ (Yb) $\rightarrow$ $^4F_{9/2}$ (Er) + $^2F_{7/2}$ (Yb)) and ET3 ($^4F_{7/2}$ (Er) + $^2F_{7/2}$ (Yb) $\rightarrow$ $^4I_{11/2}$ (Er) + $^2F_{5/2}$ (Yb)) processes, respectively.

Acknowledgment. This project is supported by the Foundation of Ministry of Education for Training Elitist Project of the Century, and the Doctoral Project Foundation of the National Education Committee of China (No. 20010358016).

References and Notes

(1) Lin, H.; Meredith, G.; Jiang, S.; Peng, X.; Luo, T.; Peyghambarian, N.; Yue-Bun Pun, E. *J. Appl. Phys.* **2003**, *93*, 186.

(2) Oliveira, A. S.; de Araujo, M. T.; Gouveia-Neto, A. S.; Medeiros Neto, J. A.; Sombra, A. S. B.; Messaddeq, Y. *Appl. Phys. Lett.* **1998**, *72*, 753.

(3) Xu, S.; Yang, Z.; Zhang, J.; Wang, G.; Dai, S.; Hu, L.; Jiang, Z. *Chem. Phys. Lett.* **2004**, *385*, 263.

(4) Balda, R.; Fernez, J.; Arriiaga, M. A.; Fedez-Navarro, J. M. *Opt. Mater.* **2004**, *25*, 157.

(5) Man, S. Q.; Pun, E. Y. B.; Chung, P. S. *Appl. Phys. Lett.* **2000**, *77*, 483.

(6) Kanoun, A.; Jaba, N.; Mejri, H.; Maaref, H.; Selmi, A. *Phys. Status Solidi A* **2001**, *188*, 1145.

(7) Guo, H.; Li, Y.; Wang, D.; Zhang, W.; Yin, M.; Lou, L.; Xia, S. *J. Alloys Compd.* **2004**, *376*, 23.

(8) Matsuura, D. *Appl. Phys. Lett.* **2002**, *81*, 4526.

(9) Silver, J.; Martinez-Rubio, M. I.; Irel, T. G.; Fern, G. R.; Withnall, R. *J. Phys. Chem. B* **2001**, *105*, 948.

(10) Vetrone, F.; Boyer, J. C.; Capobianco, J. A.; Speghini, A.; Bettinelli, M. *Chem. Mater.* **2003**, *15*, 2737.

(11) Vetrone, F.; Boyer, J. C.; Capobianco, J. A.; Speghini, A.; Bettinelli, M. *J. Phys. Chem. B* **2003**, *107*, 1107.

(12) Capobianco, J. A.; Vetrone, F.; Boyer, J. C.; Speghini, A.; Bettinelli, M. *J. Phys. Chem. B* **2002**, *106*, 1181.

(13) Patra, A.; Friend, C. S.; Kapoor, R.; Prasad, P. N. *Appl. Phys. Lett.* **2003**, *83*, 284.

(14) Patra, A.; Friend, C. S.; Kapoor, R.; Prasad, P. N. *J. Phys. Chem. B* **2002**, *106*, 1909.

(15) Martin, I. R.; Rodriguez, V. D.; Lavin, V.; Rodriguez-Mendoza, U. R. *Spectrochim. Acta, Part A* **1999**, *55*, 941.

(16) Qin, G.; Qin, W.; Wu, C.; Huang, S.; Zhang, J.; Lu, S.; Zhao, D.; Liu, H. *J. Appl. Phys.* **2003**, *93*, 4328.
(17) Downing, E.; Hesselink, L.; Ralston, J.; Macfarlane, R. *Science* **1996**, *273*, 1185.
(18) Yi, G.; Sun, B.; Yang, F.; Chen, D.; Zhou, Y.; Cheng, J. *Chem. Mater.* **2002**, *14*, 2910.
(19) Moriarty, P. *Rep. Prog. Phys.* **2001**, *64*, 297.
(20) Zhang, W. W.; Mei, X.; Zhang, W. P.; Yin, M.; Qi, Z.; Xia, S.; Garapon, C. *Chem. Phys. Lett.* **2003**, *376*, 318.
(21) Qi, Z.; Shi, C.; Zhang, W. W.; Zhang, W. P.; Hu, T. *Appl. Phys. Lett.* **2002**, *81*, 2857.
(22) Hirai, T.; Orikoshi, T. *J. Colloid Interface Sci.* **2004**, *269*, 103.
(23) Luyer, C. L.; Garcia-Murillo, A.; Bernstein, E.; Mugnier, J. *J. Raman Spectrosc.* **2003**, *34*, 234.
(24) Blasse, G.; Grabmaier, B. C. *Luminescent Materials*; Springer-Verlag: Berlin, 1994; Chapter 4, p 71.
(25) Garcia-Murillo, A.; Luyer, C. L.; Dujardin, C.; Pedrini, C.; Mugnier, J. *Opt. Mater.* **2001**, *16*, 39.